The International Journal of Advanced Manufacturing Technology (2024) 130:3053–3063
https://doi.org/10.1007/s00170-023-12880-2

ORIGINAL ARTICLE

# Efficient net shape forming of high-strength sheet metal parts by Transversal Compression Drawing

**David Briesenick**[1] · **Mathias Liewald**[1]

Received: 30 August 2023 / Accepted: 14 December 2023 / Published online: 27 December 2023


## Abstract

In this contribution, a new forming method is presented for high-strength steel sheet metal materials called Transversal Compression Drawing (TCD). For TCD, the blankholder of the conventional deep drawing process is replaced by sliders introducing a vertical force along the blank edge. Compared to conventional deep drawing, compressive stresses are thereby superimposed in the flange area of the sheet metal material, reducing the springback of formed components and the forces required during the process. Proof of this is provided here on the basis of numerical investigations in which conventional deep drawing and TCD are compared using the example of an "S-Rail" component made from DP980. Results of these investigations reveal that with TCD a maximum reduction in springback by more than 5 mm is achieved, leading to an improvement in the component´s overall shape accuracy of more than 55%. Furthermore, frictional work is decreased by – 6.92 kJ/kg, resulting in an overall reduction of maximum forming forces by 67.4%. Besides, TCD enables a trim-free net shape forming of the final part contour in a single operation and an increased material utilization of 4.5% from coil to part. Not least, no sheet thinning occurs with TCD, whereas a maximum thinning of 12% is observed with the conventional deep drawing process.

**Keywords** High-strength sheet metal · Cold forming · Springback · Efficiency · Material saving

## Nomenclature

| | |
|---|---|
| $\alpha$ | Weighting factor flow rule |
| $\varepsilon_0$ | Swift hardening parameter |
| $\xi$ | Rate of Young's modulus reduction |
| $\sigma_i$ | Yield stress |
| $\sigma_{sat}$ | Saturation stress |
| $A$ | Elongation at fracture |
| $a$ | Strength hardening law exponent |
| $A_u$ | Uniform elongation |
| $B$ | Initial size of bounding surface |
| $b$ | Kinematic hardening factor |
| $C$ | Rate of yield surface translation |
| $E$ | Young's modulus |
| $E_0$ | Initial Young's modulus |
| $E_A$ | Saturated Young's modulus |
| $E_{hg}$ | Hourglass energy |
| $E_d$ | Damping energy |
| $E_{int}$ | Internal energy |
| $E_{int}^0$ | Initial internal energy |
| $E_{kin}$ | Kinetic energy |
| $E_{kin}^0$ | Initial kinetic energy |
| $E_{rw}$ | Rigid wall energy |
| $E_{sl}$ | Sliding interface energy |
| $E_{total}$ | Total energy |
| $h$ | Rate of evolution of the stagnation surface |
| $K$ | Strength coefficient |
| $m$ | Strain hardening exponent |
| $n$ | Hardening exponent |
| $p$ | Strength hardening law exponent |
| $R_m$ | Tensile strength |
| $r_m$ | Normal anisotropy |
| $R_{p0,2}$ | Yield strength |
| $R_{SAT}$ | Isotropic saturation stress |
| $t$ | Sheet metal thickness |
| $W_{ext}$ | External work |
| $Y$ | Initial yield stress |

## 1 Introduction

Processing sheet metal materials from ultra-high-strength steels represents a promising and economically viable approach to produce sophisticated, light-weight car body

✉ David Briesenick
david.briesenick@ifu.uni-stuttgart.de

[1] Institute for Metal Forming Technology, University of Stuttgart, Holzgartenstrasse 17, 70174 Stuttgart, Germany

structures [1]. Yet deep drawing of such dedicated high-strength steels poses a challenging task for manufacturers due to their limited formability, the high process loads during forming and the tremendous springback of formed parts [2, 3]. Springback in sheet metal forming mainly arises due to the elastic strain recovery when the formed part is released from the tool and significantly affects dimensional part quality [4]. To compensate, hot and warm stamping processes are commonly applied to achieve a global or local enhancement of formability, material properties and dimensional accuracy [5–7]. However, production efficiency of this forming technology is limited due to high cycle times as well as high process and tool costs [8].

In order to achieve high dimensional quality of components made from high-strength sheet metal materials without impairing production efficiency, various cold forming technologies have been newly implemented and further developed. In this context, controlled overforming of the sheet metal part represents a common springback compensation method for conventional deep drawing and bending processes. Here, successful springback compensation depends on the proper calculation of elastic and plastic material properties in the virtual tool surface design via finite element methods (FEM) [9–11]. As this compensation strategy considers but does not reduce springback, inaccurate numerical predictions as well as process and material fluctuations may lead to rejects and thus additional costs during part production [12].

Therefore, other strategies for reducing springback are based on geometric modifications of the part´s geometry. Here, for example, selective embossing of sidewalls or radii is used to increase part stiffness [13, 14]. But, this method requires sufficient freedom in product design.

Springback can also be reduced by mechanical methods, whereby adverse residual stresses that may occur in sheet metal components after relieving are avoided or superimposed with stresses specifically introduced during the forming process [15]. In the "Crash-Form" process, for example, detrimental bending and relief stresses in the flange and sidewall areas are avoided by omitting a blankholder [16]. In contrast, tensile stresses can be superimposed at the end of the forming process by increased blankholder forces or stake beads, leading to a homogenization of the residual stress state within the sheet metal component and thus to reduced springback, while avoiding severe sheet metal thinning [17, 18]. On contrary, compressive stress superposition was achieved with a trim-free sizing deep drawing process by Kibben et al. [19]. This two-stage process comprises a preforming operation and a subsequent calibration stage. Compared to conventional deep drawing, this minimizes springback and avoids additional part contour trimming, achieving a 15% reduction in blank size

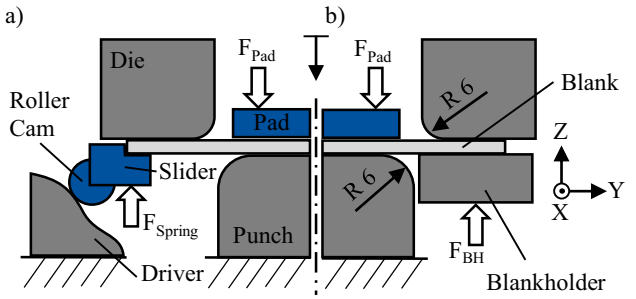


**Fig. 1** Schematic representation of the tool setup for **a** Transversal Compression Drawing (TCD) and **b** conventional deep drawing with blankholder and counter pad for the forming of open channel sheet metal parts based on [22]

for a longitudinal member. Moreover, Radonjic et al. developed a forming process with alternating draw-in of the blank to superimpose tensile and compressive stresses by a multiple bending of the sheet metal material over tool radii and thus reduce springback [20]. However, this friction controlled forming kinematic requires relatively high asymmetrically adjustable blankholder pressures.

When reviewing the state of the art for precise forming of high-strength steel sheet parts, it becomes evident that stress superposition constitutes a crucial factor in reducing springback. Yet this requires relatively high press and cushion forces during the specific forming processes, which contradicts current demands for energy-efficient manufacturing practices. In summary, the development of new cold forming processes for high-strength sheet materials should therefore not only aim to reduce springback, but also scrap losses and forming forces [21].

Based on these requirements, a single stage cold forming process called Transversal Compression Drawing (TCD) was developed by Briesenick et al. [22]. This process represents a modification of conventional deep drawing of parts with open channel geometry by substituting the blankholder with roller cam driven sliders, enabling vertical and horizontal force application along the blank edge; see Fig. 1.

The additional transverse forces applied in the flange area lead to a free buckling and rolling of the material towards the lateral punch surfaces, resulting in a continuous alternating bending stress superposition in the sidewall areas and thus to a significant reduction in springback (see Fig. 2a). In contrast, conventional deep drawing of channel shaped parts is dominated by tension superposed bending over the die radius and a subsequent unbending of the material in the sidewall areas (see Fig. 2b). When deep drawing high-strength sheet metals, which are characterized by elevated yield strength and hardening ratios, the plastification of the part cross-section is reduced, leading to a significant amount

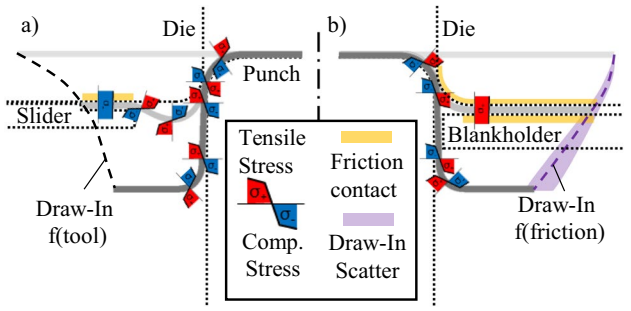


**Fig. 2** Qualitative representation of blank draw-in kinematic with the resulting alternated bending stresses and frictional contact zones for **a** the Transversal Compression Drawing (TCD) process and **b** conventional deep drawing

of elastic recovery [23]. Here, stress gradients resulting in thickness direction particularly cause a pronounced elastic contraction of the outer part skin with known springback phenomena such as sidewall curl.

The proposed tool and process setup for TCD, featuring a stroke-controlled draw-in kinematic by using flexible roller cam units, also offers potential for an efficient and robust forming process for structural sheet metal parts. Thus, blank draw-in in TCD can be predefined by direct control by the tool kinematic, whereas draw-in in conventional deep drawing fluctuates due to the frictional conditions [24]. In doing so, controlled blank draw-in of TCD enables a trim-free net shape forming of the final part contour in a single operation, thus reducing tool and scrap costs for subsequent trimming operations.

Moreover, when deep drawing high-strength sheet metals, elevated blankholder forces are often required to ensure adequate restraining forces and to achieve sufficient plastification of the part. These restraining forces are primarily affected by lubrication, counteracting blankholder forces and size of the friction contact zone in the flange area, thus resulting in relatively high energy losses during part production [25]. By contrast, the relative movement between tool and sheet metal associated with the new TCD tool design practically eliminates frictional contact areas, leading to a significant reduction in process forces.

In the following, numerical studies compare and elucidate the feasibility of the new forming process with improved draw-in kinematics. The presented numerical study builds upon previous work on material modeling of high-strength dual-phase steel DP980 [22], involving an increased sheet metal thickness ($t = 1.5$ mm) and multiple cyclic loading. Elaborated results are derived from an analysis of a double curved channel part geometry (S-Rail) and assessing the material utilization, forming energies and resulting springback through a classification against conventional deep drawing.

## 2 Characterization and modelling of sheet metal material DP980

High-strength sheet metal materials are characterized by a distinctive springback behavior after forming, which may lead to unacceptable shape deviations after the part is released from the forming tool [23]. Therefore, an accurate prediction of the expected part springback is crucial for a robust process and tool design. Regarding the test material DP980 used in the investigations, it has been found that for a precise description of the forming and springback behavior of dual-phase steel sheets, combined isotropic-kinematic hardening must be considered [26]. Furthermore, a material model based on multiple experimentally determined cyclic stress–strain curves increases the prediction quality of material behavior compared to models based on single stress–strain curves [23]. In this context, Yoshida et al. proposed a constitutive material model (Y-U model), considering the cyclic plasticity, the transient Bauschinger effect and the anisotropy of sheet metal materials [27]. Comparisons between simulation results and forming experiments have revealed that this model is particularly suitable for predicting the springback of sheet metal parts made of the dual-phase steel DP980 [28, 29]. The Y-U model was therefore also used for the investigations presented here with the dual-phase steel voestalpine CR700Y980T-DP-GI50/50-U (DP980) in sheet metal thickness of 1.5 mm. The identification of the model parameters for this sheet metal material is described in the following section based on results of several tensile, bulge, and shear tests.

### 2.1 Mechanical properties and flow curve

The characterization of elastic–plastic material properties was performed by standardized tensile tests (ISO 6892–1) with ISO II specimen shape on the universal testing machine Roell + Korthaus RKM 100. Five test repetitions were carried out at 0°, 45°, and 90° to the rolling direction and the

**Table 1** Mechanical properties and flow curve parameters for combined Swift Hockett-Sherby extrapolation rule for DP980

| Mechanical parameters | | Flow curve parameters | |
|---|---|---|---|
| $t$ [mm] | 1.5 | $\alpha$ [-] | 0.64 |
| $E$ [GPa] | 208.7 | $K$ [MPa] | 1447 |
| $Rp_{0.2}$ [MPa] | 769.8 | $m$ [-] | 0.001 |
| $R_m$ [MPa] | 1018.5 | $\varepsilon_0$ [-] | 0.11 |
| $A_u$ [%] | 6.5 | $\sigma_{SAT}$ [MPa] | 1105 |
| $A$ [%] | 11.7 | $\sigma i$ [MPa] | 722 |
| $r_m$ [-] | 0.91 | $a$ [-] | 37.23 |
| $n$ [-] | 0.1 | $p$ [-] | 0.908 |

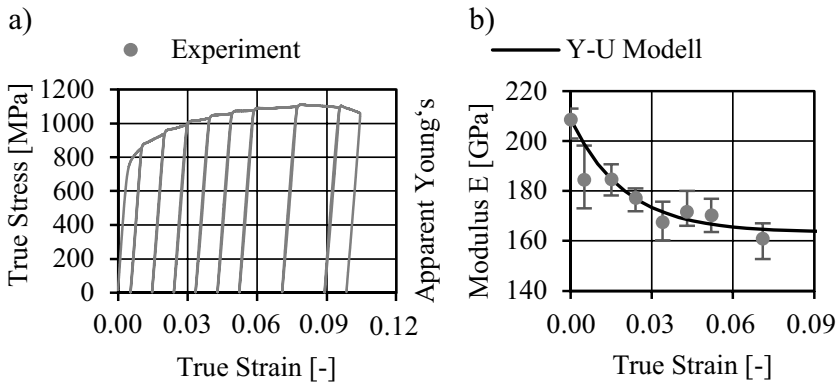


**Fig. 3** **a** Cyclic tensile tests and **b** apparent Young's modulus degradation of DP980 sheet metal material ($t = 1.5$ mm)

associated mechanical parameters were determined, as shown on the left side of Table 1.

Due to the low uniform elongation of DP980, additional hydraulic bulge tests according to ISO 16808 were performed to extend the test data at larger strains and ensure a more accurate extrapolation of the flow curve. Five repetitions were performed for these tests and the biaxial strain state was tracked by digital image correlation (DIC) measurement (GOM ARAMIS 5 M). Based on the principles of the equivalent plastic work, the biaxial stress–strain curves of the bulge tests and the uniaxial stress–strain curves of the tensile tests were used to determine a correction factor for biaxial stress–strain data. For the combined and adjusted experimental data, the extrapolation rule of Swift and Hockett-Sherby was found as the most suitable, given by Eq. (1) [30, 31]. A Matlab function for curve fitting was then used to determine the eight flow curve parameters, presented on the right side of Table 1.

$$\sigma\left(\varepsilon_{pl}\right) = (1-\alpha)\left[K\left(\varepsilon_{pl}+\varepsilon_0\right)^m\right] + \alpha\left[\sigma_{Sat} - \left(\sigma_{Sat}-\sigma_i\right)e^{-a\varepsilon_{pl}^p}\right] \tag{1}$$

## 2.2 Strain dependency of Young's modulus

Several studies have shown that increasing plastic strain during sheet metal forming results in a decrease of Young's modulus [23, 28]. To determine this strain-dependent reduction of the apparent Young's modulus, cyclic loading–unloading tests were conducted on the universal testing machine as illustrated in Fig. 3a). The tensile specimens were loaded and unloaded in several strain levels and apparent Young's modulus was determined for each loading sequence by evaluating the slopes of corresponding secants. The Y-U model considers the correlation between increasing strain and the reduction of Young's modulus, represented by the following equation [32]:

$$E = E_0 - (E_0 - E_A)\left[1 - e^{-\xi\varepsilon_p}\right] \tag{2}$$

Here, the initial Young's modulus $E_0 = 208.7$ GPa, the saturated Young's modulus $E_A = 163.4$ GPa, and the rate of Young's modulus reduction $\xi = 50.2$ were identified by a Matlab function for curve fitting.

## 2.3 Kinematic hardening

In order to determine the non-linear kinematic hardening parameters of the Y-U model, multiple cyclic shear tests were performed with modified Miyauchi specimens (see Fig. 3a) using a special shearing tool implemented on the universal testing machine. This test setup reduces the tendency of specimen buckling, which is often observed in conventional tension–compression test setups. As a result, the modified setup allows for testing at higher strains with greater accuracy [29].

To improve the quality of model prediction, several shear load cycles were tested. The shearing force was monitored by a load cell integrated into the testing machine and the shear strain was measured by the DIC system GOM ARAMIS 5 M at gauge region. The stress–strain curves derived from the five-load cycle experiment with increasing maximum strain are shown in Fig. 4b). These curves were subsequently used for the numerical parameter identification within LS-OPT. Herein, a numerical finite element simulation of a single solid element was set up in LS-DYNA, and the shearing strains were adjusted according to the experimental data. The iterative optimization strategy in LS-OPT (sequential

**Table 2** Identified kinematic hardening parameters for the Y-U model [27] of DP980 sheet metal material ($t = 1.5$ mm)

| $B$ [MPa] | $Y$ [MPa] | $C$ [-] | $m$ [-] | $R_{SAT}$ [MPa] | $b$ [MPa] | $h$ [-] |
|---|---|---|---|---|---|---|
| 595.1 | 594.1 | 44.1 | 465.6 | 189.3 | 321.3 | 0.8 |

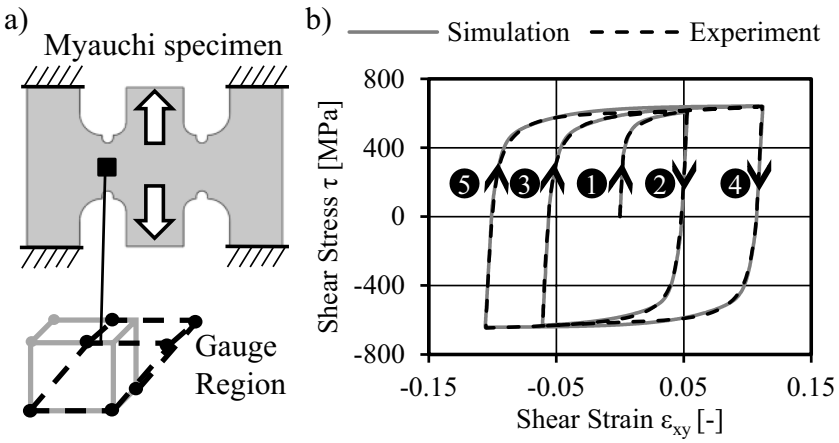


**Fig. 4** **a** Modified Miyauchi specimen and **b** curve fitting of model data based on experimental stress–strain curves

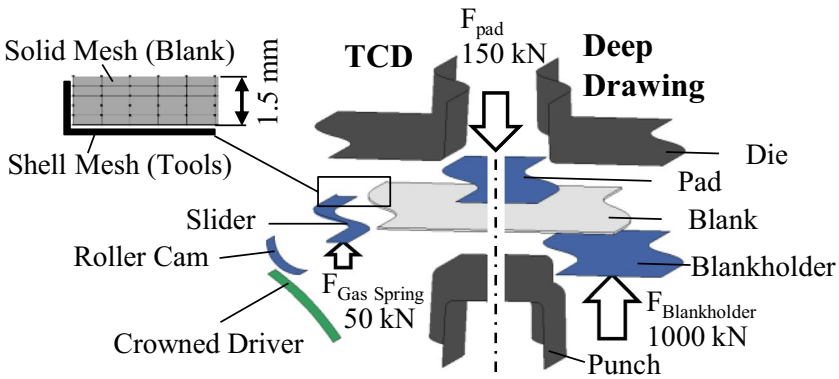


**Fig. 5** Numerical FE models of the new TCD process (left) and the conventional deep drawing of S-Rail part (right)

with domain reduction) was used to adjust the seven parameters of the Y-U model for a minimized curve matching error between simulated and experimental stress–strain curves. The obtained material parameters are listed in Table 2 and ensure a good fit between the experiment and the model, as shown in Fig. 4b.

All the parameters identified to describe the mechanical properties, the flow curve, the apparent Young's modulus and the kinematic hardening were finally implemented in the corresponding material model *MAT_125 in the FEM software LS-DYNA.

## 3 Numerical modelling of the new forming process using finite element method

The numerical modelling of the new TCD process and, in comparison, the conventional deep drawing was carried out with the commercial FE-code LS-DYNA. Both forming processes were simulated by using the explicit integration method, whereas springback calculations were performed with the implicit integration routine. The process simulations were carried out taking an S-Rail part geometry as an example. The tool surfaces derived from this part geometry were represented by rigid shell elements. Here, a typical drawing gap of + 15% of the sheet thickness was considered between punch and die face. For the conventional deep drawing process, a single action drawing operation with a fixed punch on the lower tool and a blankholder force of 1000 kN was implemented. The downward movement of the die resulted in a total drawing depth of 40 mm. A counter pad with a vertical pad force of 150 kN prevented the blank from lifting off the top surface of the punch and asymmetrical flange draw-in. The blank was modelled by volume elements with a basic edge length of 1 mm and five elements along thickness direction, as shown at the upper left side of Fig. 5. Volume elements were used, as default shell elements are limited when considering transverse contacts and 3D stress states. However, flat hexagonal volume elements may lead to locking for thin-walled structures with bending-dominant issues. To address this problem, a fully integrated S/R (selective reduced) solid formulation was used in LS-DYNA (ELFORM = − 1) for elements with poor aspect ratio, allowing for an efficient and accurate simulation [33].

Modelling the new TCD process required only minor modifications to the tool setup for the conventional deep drawing of the S-Rail geometry. First, the blankholder was substituted with L-shaped sliders applying both horizontal

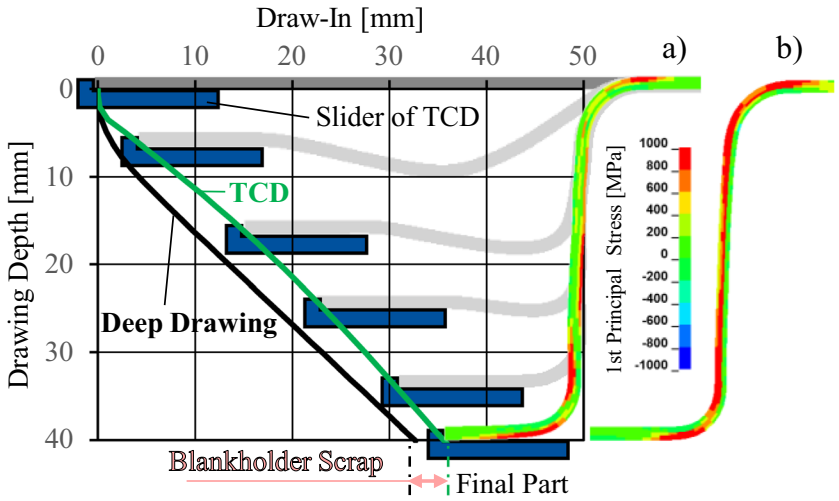


**Fig. 6** Illustration of the forming kinematic with stroke controlled blank draw-in and resulting stress state of TCD (**a**) and conventional deep drawing of S-Rail with friction controlled blank draw-in (**b**)

and vertical forces to the flange area. Second, a roller cam was modeled and connected to the sliders in order to transfer the novel stroke controlled forming kinematic by a crowned driver. Based on previous studies of the authors, a convex motion curve of the sliders, resulting in an advancing flange draw-in compared to deep drawing, was found to be beneficial for springback compensation due to stress superposition by alternated bending [22].

## 4 Results and discussion

The results of the simulations carried out were finally evaluated regarding the simulated forming kinematics, the material utilization, the resulting forming forces and energies, and the obtained part geometry. The comparison of the new forming process TCD and the conventional deep drawing based on this evaluation is presented and discussed in the following section.

### 4.1 Evaluation of material and energy efficiency

Figure 6 demonstrates the resulting draw-in of the flange in the part center area as well as the stress state of the formed part at the bottom dead center after TCD. It can be stated that the advancing flange draw-in caused by the transversal slider forces induces buckling and rolling of the sheet material and results in a successful stress superposition at the end of the TCD process due to the alternating bending (see Fig. 6a, b). Compared to the stress state after deep drawing with high stress gradients in blank thickness direction in sidewall area, the forming kinematic of TCD lead to a homogenous stress distribution in respective area. This essentially results in a significant reduction of springback, discussed in Sect. 4.2.

In addition, this tool kinematic ensures efficient net-shape forming of the final part contour, as blankholder scrap is avoided and thus trimming operations, as required for conventional deep drawn parts, can be omitted. The efficiency of high-volume production of sheet metal components depends to a significant extent on material consumption. Due to the large quantities produced here, even a small reduction in blank size can lead to considerable material savings. To this end, the required blank size for the two forming processes was compared and evaluated in terms of material efficiency and nesting losses. After an iterative adjustment of the blank size and shape for the TCD and the deep drawing process, a successful forming of the S-Rail part was achieved with both methods. In case of deep drawing, blank shape was optimized to prevent excessive draw-in in concave areas by providing a proper frictional contact area in the part flange. Here, the final blank size estimated 0.0802 $m^2$ and a weight of 0.944 kg. For the TCD process, blank shape was adjusted to reduce horizontal wrinkling and severe thickening in concave areas. In this case, final blank size amounted 0.0774 $m^2$ and had a weight of 0.911 kg. Thus, the blank size can be reduced by – 3.5% for parts formed by the TCD process.

Figure 7 presents blank nesting layouts for blank cutting on the coil. The required blank shape can either be separated from a rectangular cut-out or by an optimized nesting layout. Manufacturing of blanks by rectangular cut-outs resulted in a total material utilization of 75.4% from coil (1.217 kg per blank) to part (0.918 kg per part) for deep drawing and 76.2% for TCD with a rectangular blank mass of 1.205 kg. Cutting by an optimized blanking tool increases material utilization ratio for both processes. Here, blanking for the deep drawing process offered a material utilization of 93.1%. Nesting and trimming losses amounted 0.07 kg per part, whereas the TCD process enabled an increased material utilization of 97.4% from coil to part. As a result, the scrap per formed part can be reduced by 0.046 kg compared to

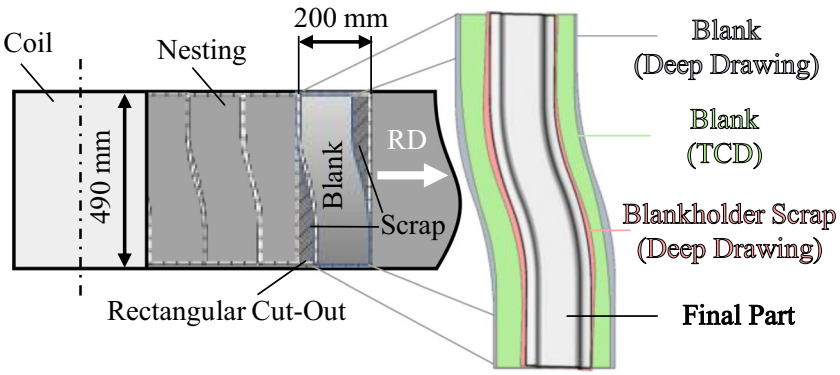


**Fig. 7** Evaluation of nesting losses and material efficiencies based on calculated blank and part sizes for TCD and conventional deep drawing

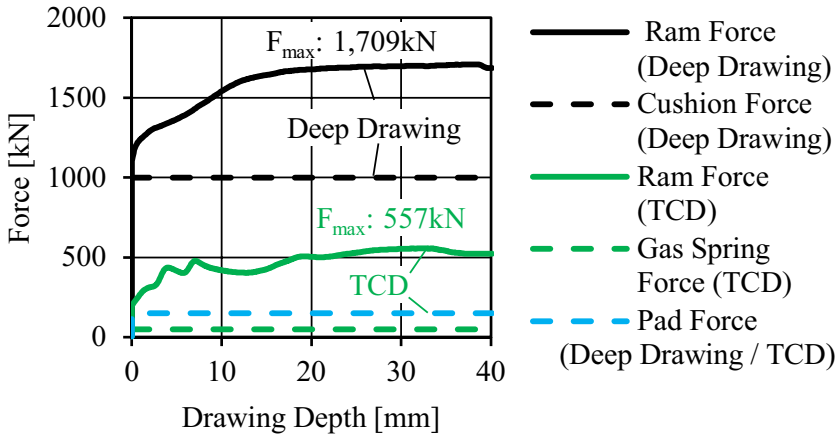


**Fig. 8** Evaluation of acting forming forces for TCD (green) and conventional deep drawing (black); see also Fig. 5

conventional deep drawing. Given an exemplary production volume of one million parts and the increased material utilization rate for TCD (+4.3%), up to 46 tons of scrap could thus be saved for the "S-Rail" part considered.

Considering future demands for a sustainable production, in addition to material savings, energy required for component manufacturing also plays a crucial role. In this respect, an evaluation of the forces acting during the conventional deep drawing and the new TCD process is shown in Fig. 8. According to this, conventional deep drawing with a blankholder force of 1000 kN and a pad force of 150 kN results in a total necessary ram force of maximum 1709 kN. Due to the minimized vertical slider forces of 50 kN and the same pad force of 150 kN, the TCD process requires a total of 67.4% less force with a maximum of 557 kN at a drawing depth of 34 mm. At this point, the previous formed kink is straightened, especially in concave part areas. The two pronounced peaks at the beginning of the forming process (drawing depths of 3.6 mm and 7.2 mm) indicate an increase of the contact zone between the blank edge and the horizontal face of the sliders.

In addition to the forming forces, the energies required for both forming processes were calculated within the numerical forming simulations and compared. Here, according to the energy balance (3) [34], the total energy $E_{total}$ is the sum of the initial kinetic $E^0_{kin}$, internal energy $E^0_{int}$, and the external work $W_{ext}$. The total energy $E_{total}$ is further defined as the sum of kinetic, internal, sliding, rigid wall, damping, and hourglassing energies. Since damping or hourglass effects are not considered in the presented forming simulation results and no kinetic or rigid wall energies are defined, the total energy balance simplifies as a sum of internal $E_{int}$ and sliding energy $E_{sl}$ (4). Thereby, internal energy $E_{int}$ includes the elastic and plastic strain energy in permanent deformation and therefore corresponds to the forming energy. The sliding interface energy $E_{sl}$ correlates with the frictional work [34].

$$E^0_{kin} + E^0_{int} + W_{ext} = E_{kin} + E_{int} + E_{Sl} + E_{rw} + E_d + E_{hg} = E_{total} \quad (3)$$

$$W_{ext} = E_{int} + E_{Sl} \quad (4)$$

For conventional deep drawing, a maximum specific energy of 12.9 kJ/kg was calculated, with a large amount occurring as frictional resistance (8.89 kJ/kg) due to the friction controlled forming process. When calculating the forming of the S-Rail part using the TCD process, a reduction in the total energy demand by 6.41 kJ/kg (− 52%) is determined. Especially the reduced frictional work (− 78%)

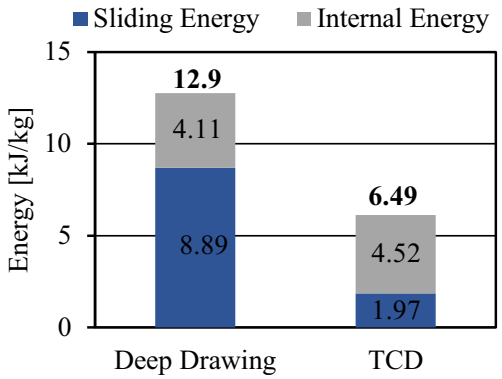


**Fig. 9** Evaluation of specific forming energies for TCD and conventional deep drawing

minimized the total sum of energy and corresponds with the reduced friction contact area associated with the TCD process; see Fig. 2. In contrast, the proportion of forming energy at 4.52 kJ/kg remained almost constant compared to the conventional deep drawing process (Fig. 9).

Based on the calculated energy values and material savings, potentials of the TCD process can be derived. Thus, it can be stated that the TCD process provides a more efficient forming method for channel parts regarding both energy and material consumption because of the net-shape forming kinematics and the reduction of frictional losses compared to conventional deep drawing processes.

## 4.2 Evaluation of the dimensional accuracy of formed parts

The dimensional part quality can be defined as the deviation between designed and manufactured part geometry. When forming structural parts made of high-strength steels, springback reduces the dimensional part quality tremendously. In the present study, springback of simulated parts was calculated by a separate implicit simulation run with the input of the part mesh as well as the stresses and strains calculated in the preceding forming simulation. Thereby, the part was fixed at the bottom area by virtual clamps to eliminate global part movement and ensure convergence of simulation. Figure 10 shows the resultant nodal displacement compared to the originally designed part for the conventional deep drawn S-Rail and the results for the TCD process.

According to the calculated simulation results, springback-related shape deviation of the S-Rail amounted to 2.06 mm on average with a standard deviation of 1.69 mm after conventional deep drawing. Due to the S-shaped part geometry with a variation of the cross section, moreover, a global twist and sidewall curl appeared. Further, bending and unbending during deep drawing caused an elastic recovery resulting in an increase of flange and sidewall angle with a maximum displacement at the flange area of 8.3 mm. The numerical predicted springback for the S-Rail part formed by TCD showed a significant reduction of springback. Overall, an average nodal displacement of 0.92 mm with a standard deviation of 0.72 mm was calculated and compared to conventional deep drawing, springback was reduced by an average of 55%. The maximum shape deviation was reduced by more than 60% and amounted to 3.3 mm, located at the convex flange area. Alternate bending by the new forming kinematic decreased stress gradients in the part cross section by bending stress superposition (see Fig. 6) and therefore reduced the elastic recovery after part release. The maximum springback in convex part areas is related to the tangential stretching of the sidewall area, resulting in an additional membrane springback. Thus, the TCD process enables an enhanced part accuracy compared to conventional deep drawing due to the beneficial stress superposition with regard to springback compensation.

Besides springback effects, manufactured sheet metal parts are often exposed to thinning effects, which can also decrease the dimensional part quality. In addition, the actual sheet thickness is important for the resistance of the component in real load scenarios. Figure 11 shows the evaluation of the actual sheet metal thickness after the S-Rails part was formed by deep drawing or TCD. The deep drawn part showed an averaged sheet metal thickness of 1.45 mm and a maximum thinning in the sidewall area of 12%. Minor thickening of 0.47% was observed in

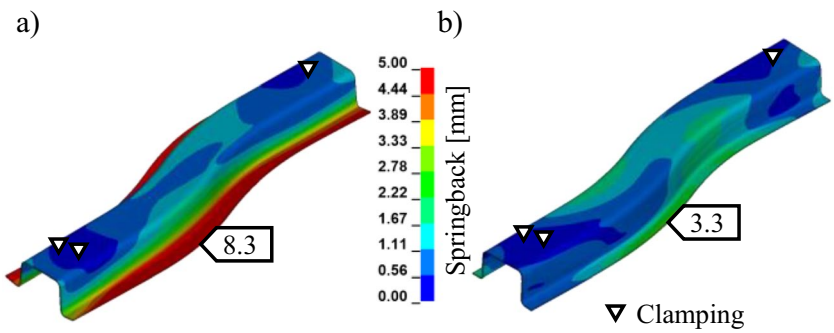


**Fig. 10** Evaluation of springback for **a** conventional deep drawing and **b** the new TCD process

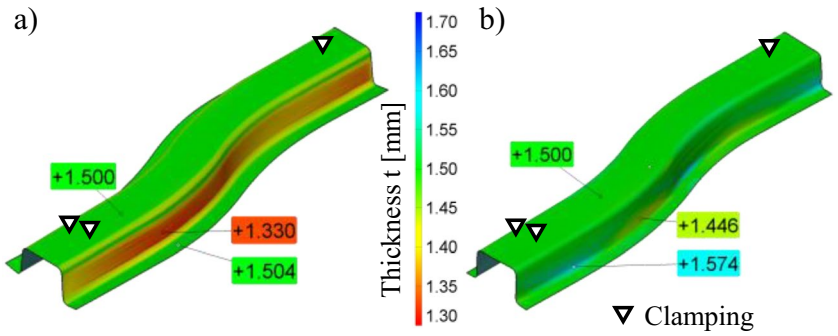


**Fig. 11** Evaluation of thinning for **a** conventional deep drawing and **b** new forming process TCD

the flange area. On contrary, the evaluation of the actual sheet metal thickness of the S-Rail part formed by TCD provided a different behavior. Due to the new forming kinematics and the absence of frictional restraining forces, almost no thinning effects were observed. Here, an average sheet metal thickness of 1.51 mm was measured and maximum of 1.57 was found in the straight part areas. The convex sidewall areas showed small thinning effects with a slightly reduced sheet metal thickness of 1.446 mm due to the tangential stretching of the material. Adding more blank material in respective areas may prevent thinning in certain areas, but it is limited by the formation of horizontal wrinkles in the final part geometry. This new type of failure, specific to the TCD process, needs to be investigated thoroughly in future studies.

## 5 Conclusion and outlook

In this contribution, a numerical feasibility study and classification of a novel cold forming process for the efficient net-shape forming of an S-Rail part geometry made of DP980 were presented. Numerical simulation results of the new process, called Transversal Compression Drawing (TCD), were thereby compared to the conventional deep drawing process in terms of material utilization, forming energies and the resulting part geometry. To ensure sufficient prediction quality of the numerical simulation, a solid element formulation and an enhanced material model for dual-phase steel DP980 was implemented, thus accounting for effects such as kinematic hardening and the strain dependency of Young's modulus.

Compared to conventional deep drawing, the draw-in of the blank edge is controlled during TCD by slider kinematics that precedes the vertical tool movement. This leads to free buckling at areas not supported by the tool and rolling of the material onto lateral punch surfaces. The consequent effect of alternated bending and the accompanying stress superposition in the sheet metal material results in a beneficial stress state with reduced springback and less frictional losses. It can be stated that for the test component "S-Rail" examined in this study, the average shape deviation due to springback was reduced from 2.06 mm for conventional deep drawing to 0.91 mm for TCD (− 55%). In addition, maximum flange displacement in the convex curved sidewall area was successfully reduced by more than 5 mm (− 60%) by the TCD process. Further analysis of the forming kinematics and the tool design with reduced frictional contact zones revealed an increase in forming energy efficiency by 55% for TCD compared to conventional deep drawing due to a reduction of the proportion of frictional losses (− 78%). The total demand for maximum press force required per stroke of 1709 kN for deep drawing was also reduced by 67.4% when forming with TCD. Further saving potentials resulted from the possible reduction of blank size and the net-shape forming of part contour without additional flange trimming operations. In this context, a study on nesting material utilization from coil to part showed scrap reduction rates of more than 4.3% due to the reduced blank size (-3.5%). These reduced nesting and trimming losses can save up to 0.033 kg per part, resulting in tons of reduced scrap for large series production. Overall, the numerical study on the new forming method TCD provided promising results for an efficient and precise manufacturing approach for high-strength sheet metal components.

Future work will focus on the experimental verification of the new forming method. Therefore, a new prototype tool to verify the numerical process model has been built and is currently undergoing testing. Here, experimental feasibility of the new forming process and parameter sensitivities to evaluate its robustness is addressed. Moreover, part properties will be analyzed and compared to deep drawn components in terms of springback, microstructure, and thinning to demonstrate the additional advantages of TCD in the manufacturing of structural components. With these findings, a subsequent transition to a group of complex industrial channel parts will be accomplished.

**Acknowledgements** The authors would like to acknowledge voestalpine Stahl GmbH for supplying the sheet metal material used in the presented investigations.

**Author contribution** All authors contributed to the study conception and design. Material preparation, data collection and analysis were performed by David Briesenick and Mathias Liewald. The first draft of the manuscript was written by David Briesenick and all authors commented on previous versions of the manuscript. All authors read and approved the final manuscript.

**Funding** Open Access funding enabled and organized by Projekt DEAL. This work was supported by Deutsche Forschungsgemeinschaft (DFG, German Research Foun-dation)–LI1556/85–1.

## Declarations

**Competing interests** The authors declare no competing interests.



## References

1. Schmitt JH, Iung T (2018) New developments of advanced high-strength steels for automotive applications. C R Phys 19(8):641–656
2. Liewald M, Radonjic R (2014) Behavior of advanced high strength steels in deep drawing processes. Ann Fac Eng Hunedoara – Int J Eng 12(1):141–146
3. Billur E, Altan PDT (2010) Challenges in forming advanced high strength steels. Int Conf New Dev Sheet Metal Forming Stuttgart 2010:285–304
4. Wagoner RH, Lim H, Lee MG (2013) Advanced Issues in springback. Int J Plast 45:3–20
5. Neugebauer R, Schieck F, Polster S, Mosel A, Rautenstrauch A, Schönherr J, Pierschel N (2012) Press hardening - an innovative and challenging technology. Arch Civ Mech Eng 12(2):113–118
6. Mori K, Maki S, Tanaka Y (2005) Warm and hot stamping of ultra high tensile strength steel sheets using resistance heating. CIRP Ann 54(1):209–212
7. Merklein M, Wieland M, Lechner M, Bruschi S, Ghiotti A (2016) Hot stamping of boron steel sheets with tailored properties: a review. J Mater Process Technol 228:11–24
8. Mori K, Bariani PF, Behrens BA, Brosius A, Bruschi S, Maeno T, Merklein M, Yanagimoto J (2017) Hot stamping of ultra-high strength steel parts. CIRP Ann 66(2):755–777
9. Gan W, Wagoner RH (2004) Die design method for sheet springback. Int J Mech Sci 46(7):1097–1113
10. Gösling M, Kracker H, Brosius A, Kuhnt S, Tekkaya AE (2011) Strategies for springback compensation regarding process robustness. Prod Eng Res Devel 5:49–57
11. Grubenmann M, Barth K, Heingärtner J, Manopulo N, Hora P, Torkabadi A, van den Boogaard T, Rösen H (2018) Analysis of yield locus description on springback behaviour of CR700Y980T-DP steel. IOP Conf Ser Mater Sci Eng 418:012108
12. Chen P, Koç M (2007) Simulation of springback variation in forming of advanced high strength steels. J Mater Process Technol 190(3):189–198
13. Weinschenk A, Volk W (2014) Decrease of springback by geometrical modification of the sheet metal part. AMR 1018:277–284
14. Radonjic R, Liewald M (2016) Approaches for springback reduction when forming ultra high-strength sheet metals. IOP Conf Ser Mater Sci Eng 159:12028
15. Tekkaya AE, Groche P, Kinsey BL, Wang ZG (2023) Stress superposition in metal forming. CIRP Ann 72(2):621–644
16. Yoshida T (2013) Springback problems in forming of high-strength steel sheets and countermeasures. Nippon Steel Tech Rep 4(10):4–10
17. Ayres RA (1984) SHAPESET: a process to reduce sidewall curl springback in high-strength steel rails. J Appl Metalwork 3:127–134
18. Roll K, Lemke T, Wiegand K (2005) Possibilities and strategies for simulations and compensation for springback. AIP Conf Proc 778(1):295–302
19. Kibben M, Bode L, Flehmig T (2018) Smartform® by thyssenkrupp - enhancement of production processes for a cost optimized cold forming of high strength steel. Int Conf New Dev Sheet Metal Form Stuttgart 2018:87–96
20. Radonjic R, Liewald M (2017) Forming with alternating blank draw-in as a new approach for springback reduction. 5th Int Conf Steels Cars Trucks Amsterdam 188
21. Horton PM, Allwood JM (2017) Yield improvement opportunities for manufacturing automotive sheet metal components. J Mater Process Technol 249:78–88
22. Briesenick D, Liewald M, Riedmueller KR (2021) New sheet metal forming process for springback reduction by continuous stress superposition. IOP Conf Ser Mater Sci Eng 1157:012030
23. Ul Hassan H (2016) Springback in deep drawing - accurate prediction and reduction. Dissertation, Technical University of Dortmund
24. Tricarico L, Palmieri M (2023) Robust design of deep drawing process through in-line feedback control of the draw. In Appl Sci 13:1717
25. Lajarin SF, Marcondes PV (2015) Influence of process and tool parameters on springback of high-strength steels. Proc Inst Mech Eng, Part B 229(2):295–305
26. Ul Hassan H, Traphöner H, Güner A, Tekkaya AE (2016) Accurate springback prediction in deep drawing using pre-strain based multiple cyclic stress–strain curves in finite element simulation. Int J Mech Sci 110:229–241
27. Yoshida F, Uemori T (2003) A model of large-strain cyclic plasticity and its application to springback simulation. Int J Mech Sci 45(10):1687–1702
28. Radonjic R (2020) Kompensationsstrategien von Rückfederungseffekten beim Umformen von hochfesten Stahlblechwerkstoffen. Dissertation, University of Stuttgart
29. Briesenick D, Liewald M, Radonjic R, Karadogan C (2019) Enhanced accuracy in springback prediction for multi-stage sheet metal forming processes. Prod Lead Edge Tech 2019:111–120
30. Swift HW (1952) Plastic instability under plane stress. J Mech Phys Solids 1:1–18
31. Hockett JE, Sherby OD (1975) Large strain deformation of polycrystalline metals at low homologous temperatures. J Mech Phys Solids 23:87–98
32. Yoshida F, Uemori T, Fujiwara K (2002) Elastic–plastic behavior of steel sheets under in-plane cyclic tension–compression at large strain. Int J Plast 18:633–659

33. Schmied C, Erhart T (2018) Updated review of solid element formulations in LS-DYNA. 15th German LS-DYNA Forum Bamberg
34. Hallquist JO (2006) LS-DYNA Theory manual. Livermore, California